

# Development of Interatomic Potentials for Supported Nanoparticles: The Cu/ZnO Case

David Mora-Fonz,<sup>\*,†</sup> Tomas Lazauskas,<sup>†</sup> Scott M. Woodley,<sup>†</sup> Stefan T. Bromley,<sup>‡,⊥</sup>  
C. Richard A. Catlow,<sup>‡,§,||</sup> and Alexey A. Sokol<sup>\*,†</sup>

<sup>†</sup>Kathleen Lonsdale Materials Chemistry, Department of Chemistry, University College London, 20 Gordon Street, London WC1H 0AJ, United Kingdom

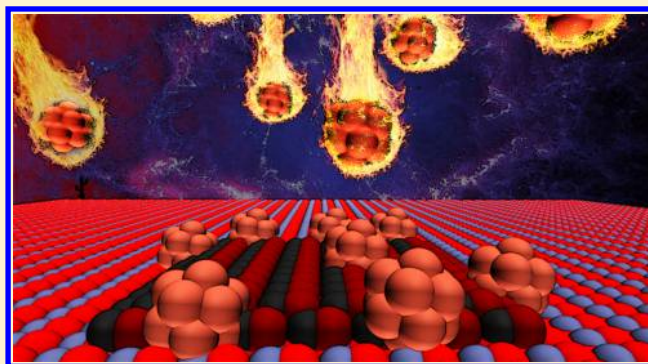
<sup>‡</sup>Departament de Ciència de Materials i Química Física and Institut de Química Teòrica i Computacional (IQTCUB), Universitat de Barcelona, Barcelona E-08028, Spain

<sup>§</sup>School of Chemistry, Cardiff University, Cardiff CF10 3AT, United Kingdom

<sup>||</sup>The UK Catalysis Hub, Research Complex at Harwell, Rutherford Appleton Laboratory, Didcot OX11 0FA, United Kingdom

<sup>⊥</sup>Institució Catalana de Recerca i Estudis Avançats (ICREA), E-08010 Barcelona, Spain

**ABSTRACT:** We present a potential model that has been parametrized to reproduce accurately metal–metal oxide interactions of Cu clusters supported on ZnO. Copper deposited on the nonpolar (10 $\bar{1}$ 0) ZnO surface is investigated using the new pairwise Cu–ZnO interatomic potentials including repulsive Born–Mayer Cu–O and attractive Morse Cu–Zn potentials. Parameters of these interactions have been determined by fitting to periodic supercell DFT data using different surface terminations and Cu cluster sizes. Results of interatomic potential-based simulations show a good agreement both structurally and energetically with DFT data, and thus provide an efficient filter of configurations during a search for low DFT energy structures. Upon examining the low energy configurations of Cu clusters on ZnO nonpolar surfaces for a range of cluster sizes, we discovered why Cu islands are commonly observed on step edges on the (10 $\bar{1}$ 0) surface but are rarely seen on terraces.



## INTRODUCTION

The Cu/ZnO system is of great interest in the chemical industry due to its wide use in the synthesis of methanol,<sup>1–9</sup> methanol steam reforming,<sup>10</sup> and water–gas shift reaction.<sup>11</sup> The production of methanol was estimated to be 65 million tonnes per year in 2013.<sup>12</sup> Moreover, the number of applications and uses for ZnO ranges from electronics to catalysis,<sup>42–45</sup> and, recently, solar radiation absorption applications have been suggested through SiC sodalite cages inside a ZnO cage.<sup>46</sup> Because of its commercial use, this system has been widely studied both experimentally<sup>1,7,8,10,11,13–25</sup> and theoretically,<sup>26–38</sup> with an emphasis on copper deposition on the ZnO polar surfaces, which show high catalytic activity in the methanol synthesis process. However, the nonpolar ZnO surfaces make up ca. 80% of the total surface area,<sup>39</sup> and are easier to model as they do not present a dipole moment across the slab nor show strong atomic reconstructions,<sup>40,41</sup> which makes them ideal to study the growth of Cu on ZnO surfaces. In this study, we develop and apply a new interatomic potential (IP)-based model for the Cu/ZnO system that matches experimental observations and is proposed for future modelling work on its complex physicochemical properties.

Experimentally, STM studies by Dulub et al.<sup>21</sup> and Patterson et al.<sup>22</sup> have revealed the morphology of Cu supported on the (10 $\bar{1}$ 0) ZnO surface. In agreement with earlier work,<sup>21,47,48</sup> clean ZnO surfaces were found to exhibit a high density of steps, running mostly along the [001] and [1 $\bar{2}$ 0] directions. In the following discussion, we identify steps by their normals in the surface plane, that is, normal to the direction in which the step runs. The stability of these features has been demonstrated in our recent work<sup>40</sup> using a combination of IP and density functional theory (DFT) based methods. Upon deposition on the (10 $\bar{1}$ 0) ZnO surface, Cu nucleates (at low coverages of 0.025–1 monolayer (ML)) in three-dimensional (3D) structures.<sup>21</sup> Dulub et al.<sup>21</sup> report the relative stability of these supported Cu clusters as follows: the [1 $\bar{2}$ 0] steps > the terraces > the [001] steps. The observed Cu clusters have a round shape with a 6–9 Å height (2–3 Cu atomic layers) and a 15–40 Å diameter. For medium Cu coverages (0.05–0.5 ML), the concentration of clusters increases faster than their average size. Didziulis et al.<sup>24</sup> observed Cu wetting (laminar growth) of

Received: May 10, 2017

Revised: June 27, 2017

Published: July 5, 2017

the polar (000 $\bar{1}$ ) ZnO surface up to 1 ML using X-ray photoelectron spectroscopy; they also concluded that similar behavior would probably be shown by the (10 $\bar{1}$ 0) and (0001) ZnO surfaces. For low Cu concentrations, isolated atoms or small islands have been seen on all surfaces. In an early study using high-resolution transmission electron microscopy,<sup>49</sup> a number of defects in the ZnO bulk were observed, which were attributed to clusters of Cu atoms in the ZnO structure that adopt an octahedral shape and are stabilized by residual carbonate groups.

Photoelectron experiments show that at low Cu coverages, there is a downward ZnO electronic band bending, which is attributed to electronic transfer from Cu to ZnO,<sup>23,24</sup> whereas at high Cu coverages, the ZnO band bending disappears. DFT calculations<sup>35,50</sup> indicate that Cu atoms interact strongly with the ZnO surface, becoming positively charged. This charge transfer was also corroborated by a hybrid DFT study by Hellström et al.<sup>32</sup> of small Cu<sub>*n*</sub> clusters (*n* ≤ 9) on the (10 $\bar{1}$ 0) ZnO surface. In this study it was concluded that even-numbered clusters are always charge-neutral, while odd-numbered clusters can become positively charged by donation of an electron to the ZnO conduction band. Cheng et al. reported that Cu atoms become slightly positive on the ZnO (10 $\bar{1}$ 0) surface using COMB2 potentials,<sup>33</sup> with values no higher than 0.11*e*, whereas the application of revised COMB3 potentials<sup>51</sup> yielded values between 0.55*e* and 0.63*e*. The latter is in better agreement with their DFT calculations (values between 0.32*e* and 0.55*e*). As mentioned, charge transfer from Cu cluster to the surface, in the electronic theory, implies an electron transfer from Cu to the conduction band of ZnO. Subsequently, a small radius electron polaron is stabilized by the positively charged Cu adsorbate on the ZnO surface. We note that both hybrid DFT and COMB2 and -3 methods encounter major difficulties in dealing with essentially one-electron charge-transfer processes, and an accurate description of this is still a major challenge. Whereas the former would typically have insufficient cancellation of self-interaction errors, the latter are not designed to deal with quasi-free electrons. Thus, both methods meet fundamental challenges in the description of charge transfer processes in this system. In this study, we neglect the possibility of such charge transfer, which deserves to be a topic of a separate investigation.

We note that Cu<sup>+</sup> and Cu<sub>2</sub><sup>+</sup> species are formed during the synthesis of Cu/ZnO catalysts, and may dissolve into and be stabilized within the ZnO bulk.<sup>6,52–56</sup> On ZnO polar surfaces, a number of studies by Jansen, Batyrev, and co-workers<sup>57–59</sup> have reported a Cu structure covered by ZnO for Cu/ZnO-based catalysts. The best match to experimental data suggested by Jansen et al.<sup>57</sup> for the active sites of the Cu/ZnO/SiO<sub>2</sub> catalyst would result from migration of ZnO species to the top of Cu nanoclusters with a formation of (partly) oxidized Cu in a Cu(I)/ZnO surfaces and O vacancies present.

Generally, nanoclusters studies focus on their stability in the gas phase; whereas in industrial applications (in particular, heterogeneous catalysis), such materials are stabilized either on or in a supporting macroscopic material (e.g., a surface). High activity of supported nanocluster calculations is commonly attributed to nanocluster–surface interactions. Accurate models of such structures are crucial for the development and understanding of new catalytic materials and mechanisms of heterogeneous catalysis. In theoretical modeling, the most common approach to study these systems is by placing the gas-phase clusters in their ground states (global minima, GM, on a

predefined energy landscape) on the surface and allowing all of their ions to relax. Recently, however, it has been shown<sup>60–62</sup> that this approach might not result in the most thermodynamically stable supported structures due to the key role of cluster–support interactions, even when the number of atoms in the cluster is small. Global optimization techniques provide a more reliable way to identify the GM of interest (see, for example, ref 63) and, therefore, are employed in our study.

Although our ideal method of choice, global optimization, is very powerful, it is also very expensive, as it requires evaluation of energy of numerous structures, which, at high levels of theory, such as DFT methods, becomes unfeasible. For example, in surface science, the number of possible relatively low energy configurations even of a medium sized nanocluster (10–30 atoms) on a surface usually exceeds 10<sup>3</sup>–10<sup>4</sup> (roughly a product of the number of gas-phase local minima and the number of symmetry unique accessible surface sites), whose geometry it would be impossible to optimize at a hybrid DFT level on a current routine basis. Accurate IP methods can, however, provide a very good first approximation to the structure and energetics of a material. Moreover, recently, these methods together with ab initio approaches have been used to calculate bulk ionization potentials and band alignments of oxides from 3D periodic calculations.<sup>64,65</sup> These techniques have a low computational cost, and allow us to sample a substantial representative portion of the potential energy landscape in a reasonable amount of time. The lowest energy structures on the IP landscape can be selected as candidates for refinement with an ab initio method. IP are also useful in the study of large systems (>1000 atoms), which are required for modeling Cu growth on nonpolar ZnO surfaces. We note that, previously, the search for the thermodynamically most stable supported metal nanoparticles has been a target of a number of global optimization studies,<sup>60,61,66</sup> which take into account the cluster–surface interaction during the global optimization search. These techniques are, however, often limited either by the computationally feasible model size or by the level of accuracy that can be achieved, leaving substantial room for improvement. Previous attempts include the study of gold clusters on MgO(100) using genetic algorithms along with a two-stage DFT optimization,<sup>60</sup> modeling of metal clusters on MgO surfaces using a combination of ab initio and semi-empirical methods,<sup>61</sup> and simulations of Cu nanoparticles on SiO<sub>2</sub>, TiO<sub>2</sub>, and ZnO surfaces using charge-optimized many-body potentials coupled with a GA.<sup>66</sup> The latter study that is most pertinent to our work has also investigated an interaction between Cu<sub>55</sub> and ZnO, but their results are difficult to assess and compare to, as their authors have chosen an idealized bulk-terminated model of a polar surface of ZnO, which cannot be realized in nature and has several artifacts.

Prior to this work, interatomic potentials have also been developed to study the Cu/ZnO system and to our knowledge, there are only three Cu/ZnO IPs reported previously. The first was created to study large Cu nanoclusters using a newly developed neural network potential.<sup>67</sup> However, the authors stated that the published potentials were not expected to work well for all Cu/ZnO applications, with open challenges for the neural network method, and further improvement was in progress. Next, Cheng et al.<sup>33</sup> have reported second-generation charge-optimized many-body potentials (COMB2) to model the Cu/ZnO system, which, however, provided erroneous ZnO “cleavage” energies, predicting the polar surfaces to be the most stable. Using a revised set of potentials (COMB3),<sup>51</sup> the

authors found the nonpolar (10 $\bar{1}0$ ) ZnO surface to be the most stable, and the polar surface to have the largest cleavage energy, with a favorable comparison to earlier DFT work. We note, however, that the surface model (an ideal clean termination) employed to calculate the cleavage energies for the polar ZnO surfaces is inappropriate, because it necessitates electron transfer between the opposite polar surfaces as the stabilization mechanism for these ZnO polar surfaces, for which there is no experimental evidence<sup>68,69</sup> and calculations yield higher surface energies as compared to the ionic reconstruction.<sup>70,71</sup> This new generation of potentials has been also used in other systems including TiN,<sup>72</sup> TiO<sub>2</sub> and Ti,<sup>73</sup> Si/HfO<sub>2</sub>,<sup>74</sup> and Cu/SiO<sub>2</sub>.<sup>75</sup> Furthermore, methodologically close, reactive force fields (ReaxFF) potentials have been suggested to study multi-component systems with applications to metal-based heterogeneous systems, such as Cu/ZnO.<sup>76</sup> ReaxFF potentials have been applied to date in the study of ZnO/water<sup>77,78</sup> and Cu/Cu<sub>2</sub>O/water systems.<sup>79</sup> To our knowledge, however, a ReaxFF IP has not been yet used to study the Cu/ZnO system.

In this Article, we report new Cu–ZnO IP that are validated via a comparison with DFT/GGA surface calculations, and applied to study the morphology of Cu clusters on (10 $\bar{1}0$ ) ZnO surfaces. Our new Cu/ZnO IP demonstrate consistently good performance in a robust prediction of low energy structures when compared to DFT. We show that a commonly employed technique of dropping clusters onto the surface does not always provide the lowest energy structure, where symmetrical restrictions for the wetting are present. We also present the first theoretical proof of the higher stability of Cu nanoclusters occupying preferentially a position over the step edge on the nonpolar ZnO (10 $\bar{1}0$ ) surface.

Following this introduction, our Article describes the following: first, the methodology including an outline of the IP fitting and of the methods used throughout this work; second, our results, where we highlight the main differences between IP and DFT GM Cu<sub>n</sub> clusters (3 < n < 13) generated by an evolutionary algorithm (EA), a genetic algorithm with phenotype move class operators, in particular,<sup>80</sup> and third, we introduce global optimization techniques applied to the growth of Cu on (10 $\bar{1}0$ ) ZnO surface, after which the stability of large nanoparticles on (10 $\bar{1}0$ ) step edges is explored.

## METHODS AND COMPUTATIONAL DETAILS

This work is based mainly on IP methods, which, however, have been calibrated against data from standard ab initio calculations. Hence, details of these latter calculations are outlined briefly below, while the molecular mechanical methods employed are subsequently discussed in detail.

**Periodic Ab Initio Calculations.** All of the electronic structure calculations were performed using the periodic plane-wave Vienna Ab-initio Simulation Package (VASP)<sup>81,82</sup> employing a generalized gradient approximation (GGA) PBEsol functional.<sup>83</sup> The interactions between core (Zn:[Ar], O:[He], and Cu:[Ar]) and valence electrons were described with the projector augmented wave (PAW) approach.<sup>84,85</sup> The ZnO surface models employed were those of the nonpolar (10 $\bar{1}0$ ) and (11 $\bar{2}0$ ) surfaces. A kinetic energy cutoff of 700 eV was sufficient to converge the bulk lattice energy (four atoms unit cell) to less than 1 meV. Surface supercell sizes of (4 × 4) (320 atoms) and (4 × 3) (240 atoms) with a vacuum gap of 18 Å were found to be large enough to avoid the effects of spurious interactions between periodic images. For the (10 $\bar{1}0$ ) ZnO surface, a 2 × 1 × 1  $\Gamma$  centered *k*-point mesh was used for

the (4 × 4) supercells and 2 × 2 × 1 for the (4 × 3), respectively. When an atomic relaxation was performed, the forces on all ions were converged to less than 0.02 eV Å<sup>-1</sup>. DFT calculations were used to (i) generate the data, to which the IP are fitted, and (ii) refine the Cu<sub>8</sub> and Cu<sub>13</sub>/ZnO structures obtained with global optimization techniques using IP as a measure of structure stability.

**Choice of IP.** The IP calculations were carried out using the General Utility Lattice Program (GULP)<sup>86,87</sup> with the polarizable shell model potentials for ZnO developed by Whitmore et al.,<sup>88</sup> and an embedded-atom model IP for Cu by Cleri and Rosato<sup>89</sup> (Table 1).

**Table 1.** Parameters of the IP Used for the Cu–Cu interactions<sup>a</sup>

A (eV)		Buckingham		C (eV Å <sup>6</sup> )	
9837.021759		$\rho$ (Å)		0.0	
		Embedded Atom Model			
EAM functional		EAM density			
type	A	type	A	$\beta$	$r_0$
square root	1.0	Baskes	1.498176	4.556	2.556191

<sup>a</sup>Potentials taken from ref 89. The values presented in this table are a conversion from the Gupta potentials, where the repulsive part was adapted to the Buckingham potential and the many-body term to the embedded atom model. A radial cutoff of 12 Å was used for all IP.

The IP parameters representing the Cu–O and Cu–Zn interactions were fitted to a set of data comprising a series of geometries and energies obtained with periodic single-point (SP) DFT calculations of Cu<sub>4</sub> and Cu<sub>8</sub> clusters interacting with the bulk terminated nonpolar (10 $\bar{1}0$ ) and (11 $\bar{2}0$ ) ZnO surfaces. Adsorption energies were validated using a higher quality hybrid DFT test on the Cu<sub>4</sub>/(11 $\bar{2}0$ )–ZnO system.

The schematic model used to generate the training set is shown in Figures 1 and 2. For Cu<sub>4</sub>, one adsorption site on each ZnO surface was employed (Figure 1), whereas for Cu<sub>8</sub>, three different sites were chosen: two on the (10 $\bar{1}0$ ) and one on the (11 $\bar{2}0$ ) ZnO surface (Figure 2). A set of 18 SP DFT calculations for each site were used in the fitting procedure (90 SP DFT points in total). In these 18 SP calculations, only the *z* coordinate of the Cu atomic positions varies; see side views of Figures 1 and 2. The distances between the topmost ZnO surface atom and the closest Cu atom were varied in steps of 0.1 Å from 1.5 to 2.0 Å, of 0.2 Å from 2.0 to 3.0 Å, and of 0.5 Å from 3.0 to 6.0 Å. Additionally, one SP calculation was made at 9.0 Å (at the middle of the vacuum slab), which represents the Cu cluster being in the gas phase having no interaction with the ZnO slab and where the adsorption energy is set to zero, and the remaining data points are referred to this value. This methodology takes into account not only different surface atomic terminations, but also different Cu cluster morphologies: planar (Cu<sub>4</sub>) and 3D (Cu<sub>8</sub>).

Buckingham and Morse potentials (Table 2) were used to describe the Cu–O and Cu–Zn short-range interactions, respectively. The forms of the IP are:

$$E_{\text{Buckingham}} = A e^{-R/\rho} - C/R^6$$

$$E_{\text{Morse}} = D_e((1 - e^{-a(R-r_0)})^2 - 1)$$

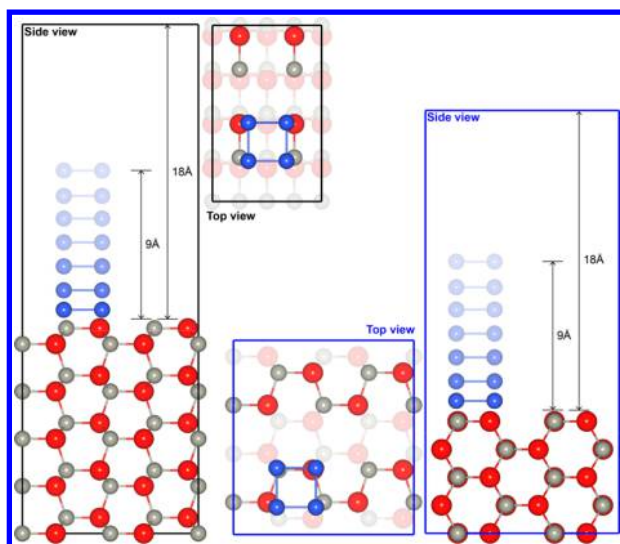


**Figure 1.** Top and side views of the  $\text{Cu}_4$ -ZnO structural model employed in fitting parameters of interatomic potentials to DFT data. The  $(10\bar{1}0)$  (black) and the  $(11\bar{2}0)$  (blue)  $(2 \times 2)$  supercell are shown. In the side views, different blue shades were used to represent the heights of the SP calculations. Blue circles are reserved for copper atoms.

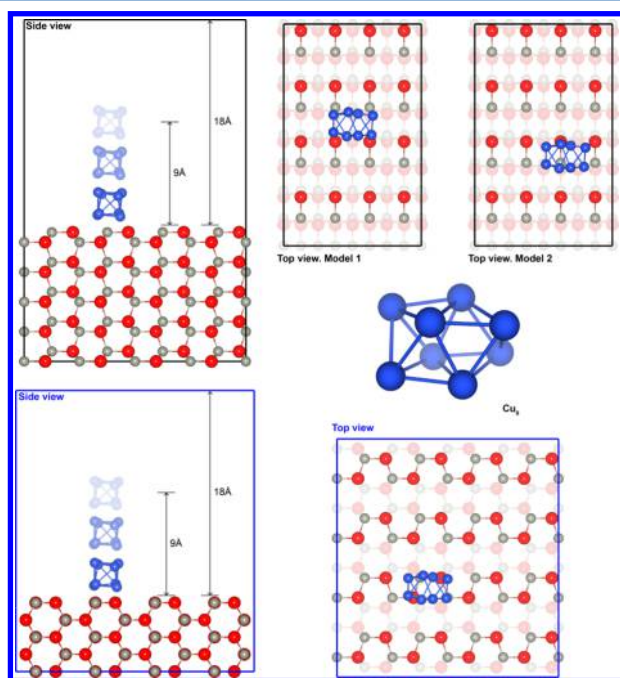


**Figure 2.** Top and side views of the  $\text{Cu}_8$ -ZnO structural model employed in fitting parameters of interatomic potentials to DFT data. The  $(10\bar{1}0)$ , in black, the  $(11\bar{2}0)$ , in blue,  $(4 \times 4)$  supercell, and the GM  $\text{Cu}_8$  cluster are shown. In the side views, different blue shades were used to represent the heights of the SP calculations. Blue circles represent copper atoms.

**Table 2.** Parameters of the IP Used for the Cu-ZnO System<sup>a</sup>

Morse	$D_e$ (eV)	$a_0$ ( $\text{\AA}^{-1}$ )	$r_0$ ( $\text{\AA}$ )
Cu-Zn	1.148402	1.7393	2.23494
Buckingham	$A$ (eV)	$\rho$ ( $\text{\AA}$ )	$C$ ( $\text{eV \AA}^6$ )
Cu-O	46.34077	0.593419	0.0

<sup>a</sup>A radial cutoff of 12  $\text{\AA}$  was used for all potentials.

where  $R$  represents the distance between the ions in question. The Buckingham potential has an intrinsic problem at short interatomic distances: the  $Cr^{-6}$  term diverges when the interatomic distance  $r$  tends to zero. To avoid this problem and noting that the  $C$  term in the Cu-O IP does not improve substantially our fit, the  $Cr^{-6}$  was excluded from the potential. Thus, the attractive Cu-Zn interaction (coordination bonding of electron-rich Cu atoms to electron-poor Zn cations) has been described using the Morse potential and the repulsive Cu-O interactions (Pauli repulsion) by the Born-Mayer term. Further details of the fitting procedure are given below.

**Interatomic Potential Fitting.** The number of atomic arrangements even for small systems such as  $\text{Cu}_n/\text{ZnO}$  ( $n \leq 13$ ) can be huge and unfeasible to study at the DFT level. On the other hand, a good IP can provide a reasonably accurate atomic structure and energy at a much cheaper computational cost: for example, one single periodic 200-atom structure can be optimized in ca. 1 h using one computer processor, whereas a calculation for the same system at the DFT/GGA level (within the VASP code) can take up to 1 day (depending on how far the initial structure is from the local minimum) using hundreds of processors. The creation of Cu/ZnO IP will help to explore the potential energy surface of this system in depth at a reasonable computational cost. The process developed to create the Cu/ZnO potentials is outlined below.

First, parameters of the Cu/ZnO potentials were fitted using relaxed  $(10\bar{1}0)$  and  $(11\bar{2}0)$  ZnO surfaces with a  $\text{Cu}_8$  cluster on three adsorption sites, which are shown in Figure 2 (54 data points); however, this procedure resulted in the Cu-Zn potential parameters dropping to zero. This behavior has been attributed to the termination of the surface slab: as shown in our recent publication,<sup>40</sup> both nonpolar ZnO surfaces show an anionic termination with strong cationic relaxation toward the bulk. Thus, it should be expected that on adsorption Cu clusters will be well separated from Zn ions and, therefore, experience only a weak interaction. Hence, relaxed ZnO atomic surface structures are not optimum to probe the interactions between Cu and Zn atoms at the DFT level. We have resolved instead to use bulk-like nonpolar ZnO surface terminations that expose the surface Zn ions to an unhindered interaction with Cu atoms.

Using a revised setup, we have retained the original 54 data points, which correspond to adsorption over the groove separating two adjacent bands of dimers on the  $(10\bar{1}0)$  surface (model 1) and on top of ZnO dimers on both surfaces (models 2 and 3); see Figure 2. A further 36 data points were added to the data including those for a planar  $\text{Cu}_4$  cluster (Figure 1), also adsorbed on top of ZnO dimers on each nonpolar ZnO surface. This refinement achieved a good balance between planar and nonplanar configurations and Cu clusters of different sizes.

Figure 3 shows the adsorption potential energy profiles as calculated with DFT and the new Cu-ZnO potentials (Table 2). Good agreement between the IP and DFT calculations is clearly achieved. When compared to DFT, our IP matched the equilibrium bond length in three of the five cases with an error of  $<0.1 \text{ \AA}$  for the other two sites:  $(10\bar{1}0) + \text{Cu}_8$  model 2 and  $(11\bar{2}0) + \text{Cu}_4$ . Moreover, a good match of the energy depth is achieved in all cases.

**Global Optimization of Cu/ZnO Structures.** The new Cu-ZnO IP were used in an unbiased Monte Carlo exploration of the energy landscape for  $\text{Cu}_n$  ( $n = 8, 13$ ) on the  $(10\bar{1}0)$  ZnO surface with the Knowledge Led Master Controller (KLMC) code,<sup>80,90,91</sup> leading to the discovery of the best candidates for

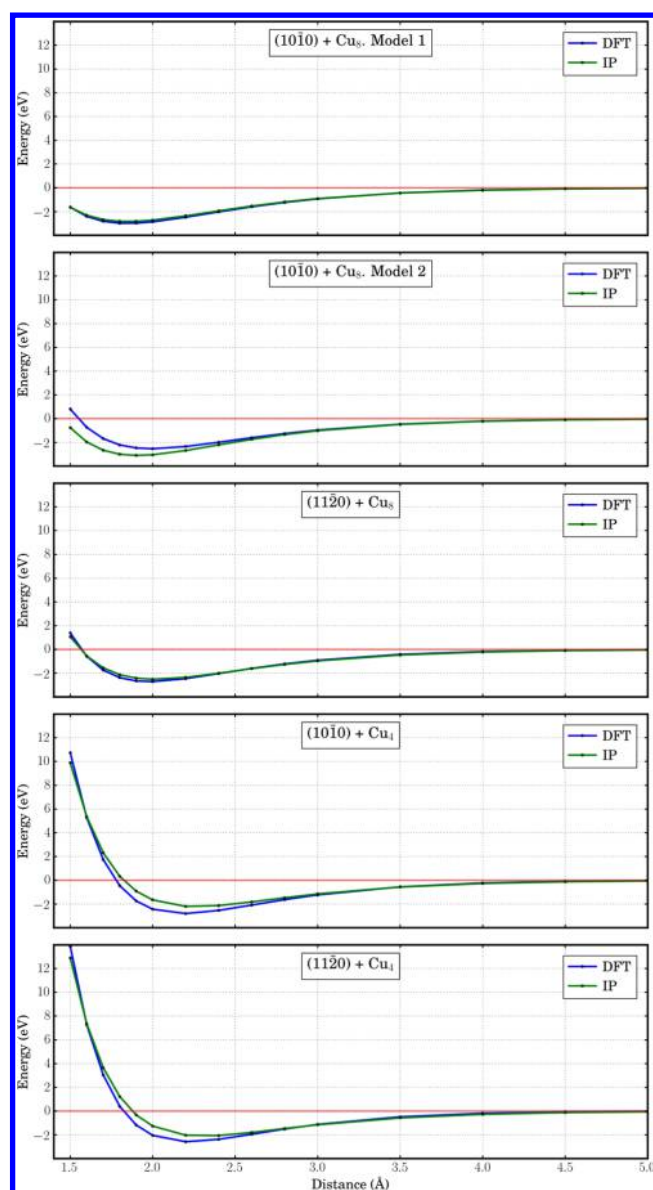


**Figure 3.** Potential fitting curves. Blue and green lines show the adsorption energy data points using DFT and IP, respectively. From 5 to 9 Å, all of the curves remain flat to the naked eye.

GM. The Monte Carlo routine was used to perform this task, which created 10 000 different  $\text{Cu}_n/\text{ZnO}$  structures by swapping Cu ions over a given lattice mesh. A ZnO slab of size  $(4 \times 3)$  and a depth of 5 double atomic layers (240 atoms) was employed with the restriction that only Cu atoms are fully relaxed. The Cu mesh used was 3 atomic layers (41 atoms) in a  $(4 \times 4)$  supercell of the (110) Cu surface, where the closest Cu atoms is at ca. 2.5 Å above the topmost ZnO surface atom (Figure 4). The five lowest energy  $\text{Cu}_8/\text{ZnO}$  and twenty  $\text{Cu}_{13}/\text{ZnO}$  configurations were refined with a DFT approach. An analysis of the difference in structure and stability between DFT and IP (for  $\text{Cu}_8/\text{ZnO}$ ) is presented below. Furthermore, we show the reliability of predicting low energy structures by making a comparison between the lowest energy  $\text{Cu}_{13}/\text{ZnO}$  energy configurations as predicted with IP and refined by DFT. Having tested the reliability of our Cu/ZnO IP, we proceed to search for the lowest energy  $\text{Cu}_{3-7}/(10\bar{1}0)\text{-ZnO}$  structures at the IP level, and the settings are presented in Table 3.

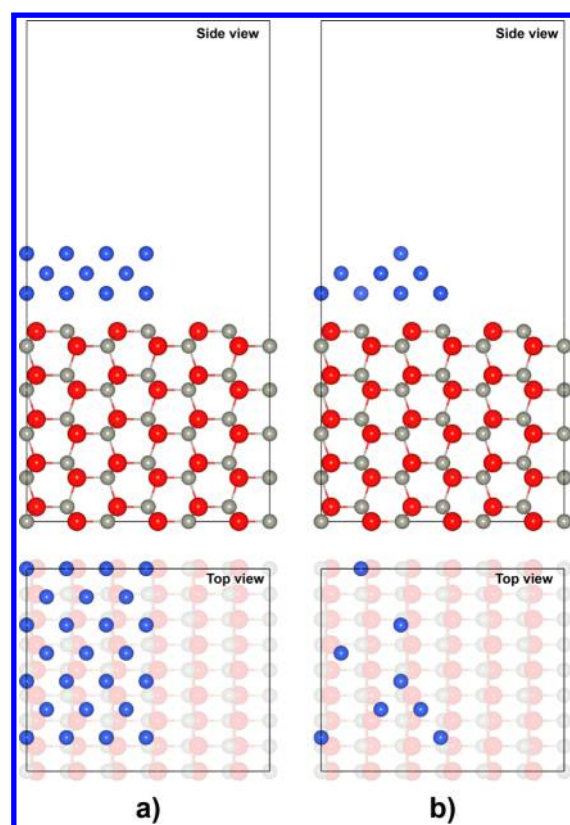


**Figure 4.** Graphical representation of the global optimization process used within KLMC. Part (a) shows the 5 double-layer  $(4 \times 3)$  ZnO surface with 3 atomic layers of a  $(4 \times 4)$  supercell of the (110) Cu surface on top of it. This picture shows 41 Cu lattice positions from which 8 will be occupied. (b) A structure example created by KLMC after the swapping process with 8 Cu occupied lattice positions.

**Table 3.** Global Optimization Settings<sup>a</sup>

$\text{Cu}_n$	atomic Cu layers	number of lattice positions	number of samples
3	1	16	1000
4	2	25	1000
5	2	25	2000
6	3	41	3000
7	3	41	3000
8	3	41	10000

<sup>a</sup>Headings are the number of Cu atoms deposited on the ZnO surface, atomic Cu layers and number of lattice positions belonging to the (110) Cu surface mesh, and number of the global optimization samples. See Figure 4.

To speed up the energy minimizations during the global optimization calculations, we have studied different aspects that could modify the Cu/ZnO atomic structure: (i) the effect of the ZnO slab relaxation on the structure of the Cu cluster; (ii) the reduction of the ZnO supercell from  $(4 \times 4)$  to  $(4 \times 3)$ ; and (iii) the Cu/ZnO optimized structure when two different initial configurations are used.

In Figure 5 we compare a fully optimized atomic structure of  $\text{Cu}_8/\text{ZnO}$  with the structure of the same cluster adsorbed on a frozen bulk terminated ZnO surface. The two configurations differ little, with only noticeable changes in the ZnO slab where Zn ions undergo strong inward relaxation as in ref 40. The effect of the ZnO slab relaxation on the  $\text{Cu}_8$  atomic structure is small, thus allowing us to reduce substantially the computa-

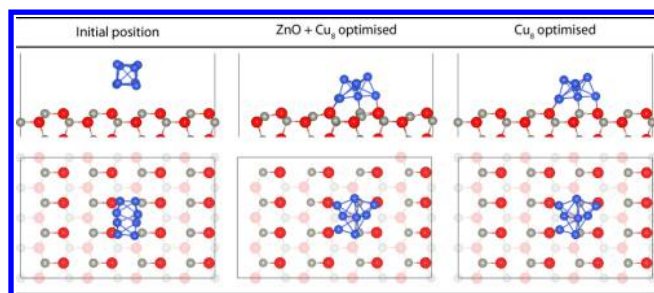


**Figure 5.** Top and side views of the initial and optimized  $\text{Cu}_8/\text{ZnO}$  structures. The border lines represent the  $(4 \times 4)$  supercell. All ions were allowed to relax in the figures at the center, whereas in the figures on the right the ZnO atoms were held fixed.

tional cost in our subsequent calculations by keeping the ZnO substrate fixed.

Figure 6 displays a reduced  $(4 \times 3)$  supercell of the  $(10\bar{1}0)$  ZnO surface model with a  $\text{Cu}_8$  cluster sited on top in two

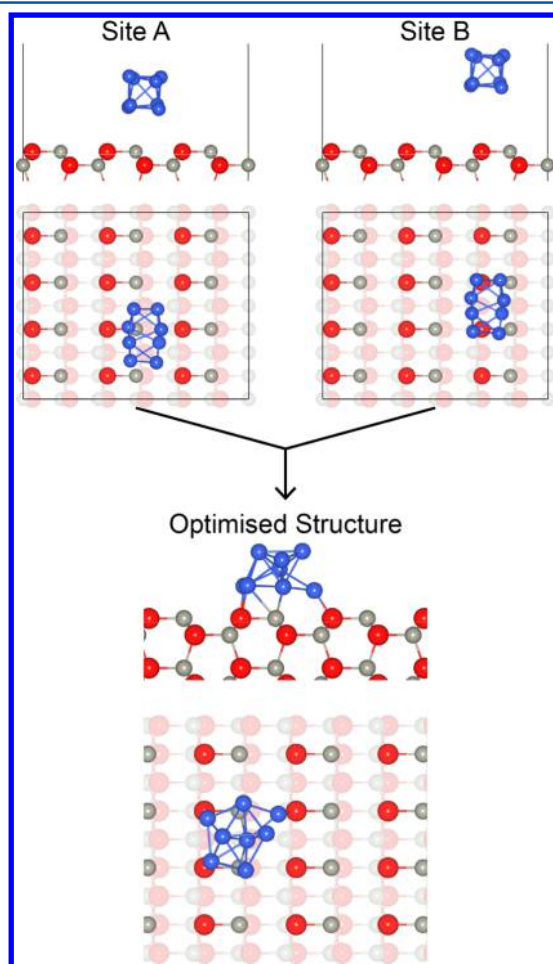


**Figure 6.** Top and side views of two different initial  $\text{Cu}_8/\text{ZnO}$  structures. The black lines represent the  $(4 \times 3)$  supercell. Both structures optimized in the same final structure shown at the bottom of the figure.

different positions (see top views), which will allow us to investigate points (ii) and (iii) above. Upon optimization, both clusters adopt the same atomic structure. Because the  $(10\bar{1}0)$  ZnO slab does not have many morphologically different sites, and the  $\text{Cu}_8$  is big enough to cover most of them, we would

expect that this optimized structure or its symmetry equivalent will always be found using different starting points. We notice, moreover, that the difference in adsorption energy per Cu atom between the  $(4 \times 4)$  and  $(4 \times 3)$  supercells, for the  $\text{Cu}_8$  cluster shown in Figure 5, is 0.0075 eV and the optimized structure is the same. Therefore, neither the reduction of the ZnO supercell to  $(4 \times 3)$  nor the use of different initial configurations affects the DFT results. Consequently, in our global optimization calculations, we use a  $(4 \times 3)$  supercell with the ZnO slab fixed.

**$\text{Cu}_n$  ( $3 \leq n \leq 13$ ) Global Minima Gas-Phase Clusters As Predicted with EA.** The global minimum structures of the gas-phase Cu clusters on the IP energy landscape was predicted using an improved Lamarckian evolutionary algorithm within the KLMC software suite.<sup>80</sup> The new algorithmic features in the software include topology-based prescreening and the new mutation classes, which makes it more robust as compared to the classical approach. It has proven to be a powerful and reliable tool for structure prediction of nanoclusters and their analysis. The main parameters for the simulations in this work, including the population size, number of iterations, and simulation box size, are given in Table 4, whereas other settings were kept the same as in the original publication.<sup>80</sup>

**Table 4.** Evolutionary Algorithm Settings for the Search of Gas-Phase GM  $\text{Cu}_n$  ( $3 \leq n \leq 13$ )

$n$	population	iterations	box size (Å)
3	20	50	3
4	50	100	3
5	50	100	3
6	50	150	3
7	50	150	3.5
8	50	150	3.5
9	50	200	4
10	50	200	4
11	50	200	4
12	75	300	4.5
13	75	350	4.5

**Cu Growth on Step Edges of the  $(10\bar{1}0)$  Surface.** As noted earlier, copper deposition, at room temperature, on clean nonpolar  $(10\bar{1}0)$  surfaces has been studied by Dulub et al.<sup>21</sup> using STM techniques. Cu nucleates in 3D structures with a very well-defined stability order: along the  $(1\bar{2}10)$  steps (step edges perpendicular to the  $[1\bar{2}0]$  atomic row direction) > on the terraces > along the  $(0001)$  steps. The average Cu cluster morphology observed is a 3D shape with 6–9 Å in height (2–3 Cu layers) and 15–40 Å in diameter.<sup>21</sup> To account for such dimensions, copper clusters with more than 100 atoms are needed, and as the cluster size increases so does the difficulty in finding the GM. Moreover, modeling accurately a system for those Cu dimensions would need a ZnO slab model with more than 10 000 atoms. As pointed out by Patterson et al.,<sup>22</sup> examining Cu clusters of the size seen in experiment<sup>21,22</sup> is not practical at the DFT level. However, IP methods can provide a basis for understanding the Cu features observed on the  $(10\bar{1}0)$  surface.

For practical purposes, we have used the EA technique used above for small Cu clusters to search for the  $\text{Cu}_{55}$  GM at the IP level. We have found the same structure as Darby and co-workers;<sup>92</sup> this cluster has a two-shell centered icosahedral structure; see top left-hand side in Figure 7. The  $\text{Cu}_{55}$  GM structure resembles a sphere ca. 8.5 Å in diameter, which we

consider to be a good first approximation to the clusters observed by Dulub et al.<sup>21</sup>

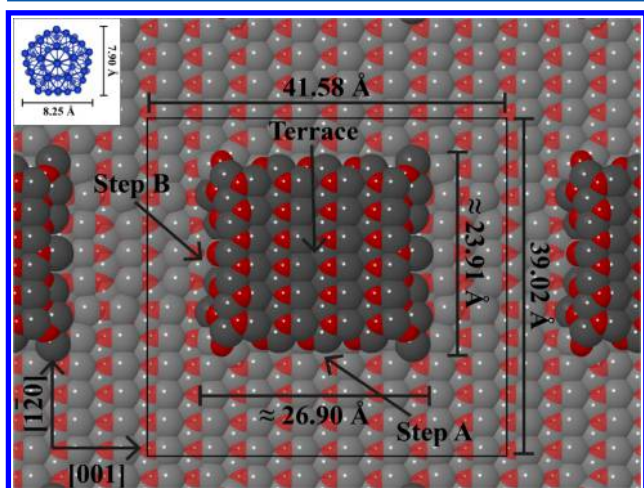


**Figure 7.** Top view of Cu adsorption sites, as suggested by Dulub et al.,<sup>21</sup> on the (10 $\bar{1}$ 0) ZnO surface. Zn and O ions forming the terrace are shown with darker colors. Simulation unit cell, (12  $\times$  8), is represented by the black square. Cu<sub>55</sub> GM cluster used in the simulations is shown in the top left-hand side.

To model accurately cluster-support interactions, we built a one-sided 2D periodic surface model using a two region approach.<sup>40,86,87</sup> This method allows relaxation of the atoms in the region exposed to the vacuum, whereas the second substrate region is held fixed representing the bulk crystal. To give a good representation of the scale of the STM observations by Dulub et al.,<sup>21</sup> we constructed a (12  $\times$  8 10 $\bar{1}$ 0) ZnO surface model, with a supercell size of 39.02 Å  $\times$  41.58 Å (see Figure 7). Four ZnO layers ( $\sim$ 10.4 Å) were used in both region one and region two (more than 4000 atoms in our simulations). A graphical representation of our model is shown in Figure 7.

## RESULTS AND DISCUSSION

**Gas-Phase Global Minima Cu Clusters.** Employing high-quality IP, we can efficiently obtain a good approximation to the atomic structure of a material. Given the vast number of possible configurations to assess, a pure DFT approach is not tractable. For the Cu–Cu interatomic interactions, we have chosen to use the Gupta many-body potentials by Cleri and Rosato,<sup>89</sup> which have been widely used in a study of cluster structures, their growth and dynamics,<sup>92–95</sup> and, in particular, in the structure prediction of Cu<sub>*n*</sub> clusters (*n*  $\leq$  56) using a genetic algorithm (GA).<sup>92</sup>

Here, global minima (GM) structures for gas-phase Cu<sub>*n*</sub> clusters have been obtained using a highly efficient EA algorithm<sup>80</sup> on the IP energy landscape for sizes *n* = 3–13, respectively. The tentative GM structures are shown in Figure 8, along with their respective total energies and point symmetries. All IP global minima structures have triangular faces, and are found to have high symmetry geometries (an effect of attractive long-range forces in the Gupta potential) and are mainly based on icosahedral structures.<sup>92</sup> The larger global minima Cu structures for the Gupta potentials compare well with those obtained using different techniques.<sup>93,96–98</sup> The main difference between small Cu clusters found on the IP and DFT energy landscapes is the preference for planar structures for the latter energy landscape. Calculations show planar Cu<sub>*n*</sub> (*n*

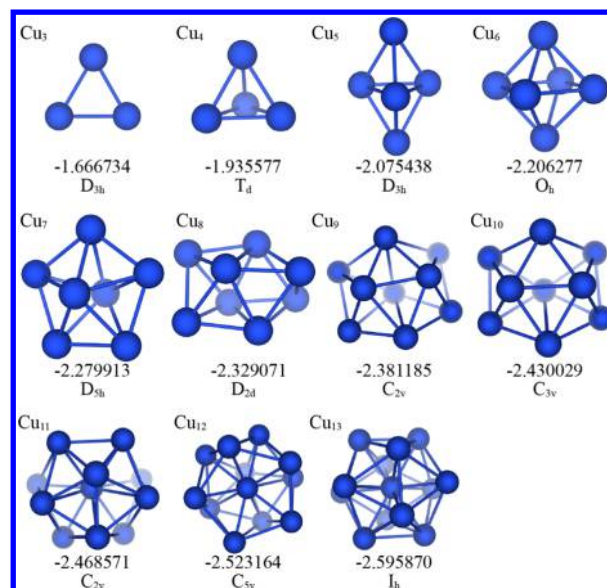


**Figure 8.** Global minima Cu<sub>*n*</sub> clusters (3  $\leq$  *n*  $\leq$  13) as calculated with the Gupta interatomic potentials.<sup>89</sup> Total energies per Cu atom and symmetry are given below each global minima found.

< 7) structures being favored at the GGA level, whereas the smallest nonplanar GM at the LDA level is found for Cu<sub>6</sub>, although only slightly lower in energy than the planar configuration found to be the GGA GM.<sup>99</sup>

**Global Optimization of Supported Clusters.** If there were negligible wetting, then we would only need to consider how best to place on the surface the GM clusters found in the gas phase. Ignoring the trivial case of one Cu atom, the gas-phase GM for Cu<sub>2</sub> is also the stable configuration on the support, as opposed to two isolated Cu atoms on the support. As wetting becomes more significant, other low energy configurations found in the gas phase may find a better match to the surface than the gas-phase GM cluster, resulting in a lower total energy. The problem of mismatch between the order of stability found in the gas phase and supported clusters exacerbated when the number of Cu atoms increases as there is typically a higher number of density of states density of other possible cluster configurations with energy similar to that of the gas-phase GM. For even stronger wetting, unstable gas-phase clusters may become stable on the support. Thus, as well as scanning for the best fit location for the gas-phase clusters, it is important also to search for other Cu configurations in the presence of the support.

Global optimization techniques were used in the search of the global minimum for each system, with a set of 10 000 different Cu<sub>*n*</sub>/ZnO (*n* = 8 and 13) structures found to be enough to find the plausible tentative global minimum. These structures were relaxed to a local IP minimum, with IP parameters taken from Whitmore et al.<sup>88</sup> (ZnO), Cleri and Rosato<sup>89</sup> (Cu), and those here (Cu/ZnO, Table 2). For Cu<sub>8</sub> (Figure 9), five of the twenty lowest energy structures were chosen for further refinement, to obtain a DFT local minima, and a more detailed analysis. For Cu<sub>13</sub> (Figure 10), the twenty lowest IP energy structures were similarly refined and analyzed. We consider that analyzing the differences between IP and DFT results for these two cases is enough to probe the accuracy of our IP models. In general, when compared to DFT, the Cu/ZnO IP results show a good agreement both structurally and

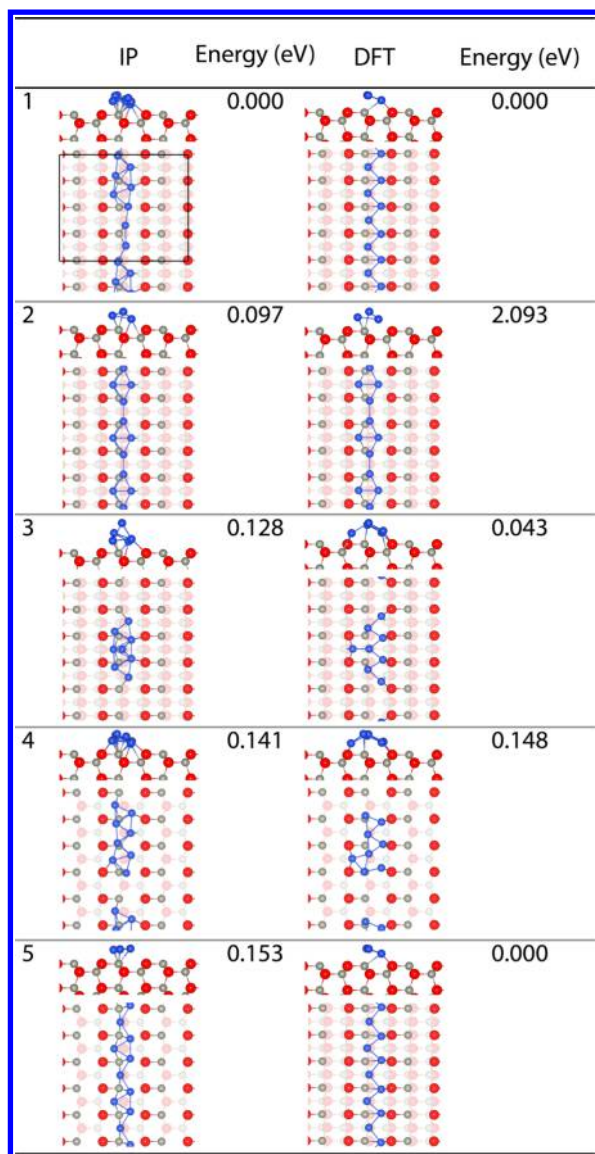


**Figure 9.** Top and side views of the five lowest energy  $\text{Cu}_8/\text{ZnO}$  structures from global optimization. On the left, the structures predicted by our new  $\text{Cu}/\text{ZnO}$  set of potentials. On the right, the structures refined by DFT. Energies are with respect to the lowest energy structure on the respective energy landscapes. The  $(4 \times 3)$  supercell is shown in the first structure.

energetically and thus proved to be a good filter for finding low DFT energy structures.

**$\text{Cu}_8/\text{ZnO}$ : A Structural and Energy Comparison between IP and DFT.** The  $\text{Cu}_8/\text{ZnO}$  case has been chosen to study the structural and energetic differences between IP and DFT; the reliability of our new set of  $\text{Cu}/\text{ZnO}$  potentials will be discussed in this section. Structurally, similarities between IP and DFT calculations are clear, and only a few significant atomic displacements are observed. The lowest DFT energy structure was found with two different IP structures. We note a preference for planar Cu structures over nonplanar. The optimized structures were found in less than 40 ionic steps in 60% of the cases, whereas placing a GM  $\text{Cu}_8$  cluster at 3 Å can take over 200 ionic steps, thus reducing the computational cost by ca. 80%. Copper atoms supported on ZnO tend to form triangular configurations, like those in gas-phase copper clusters.

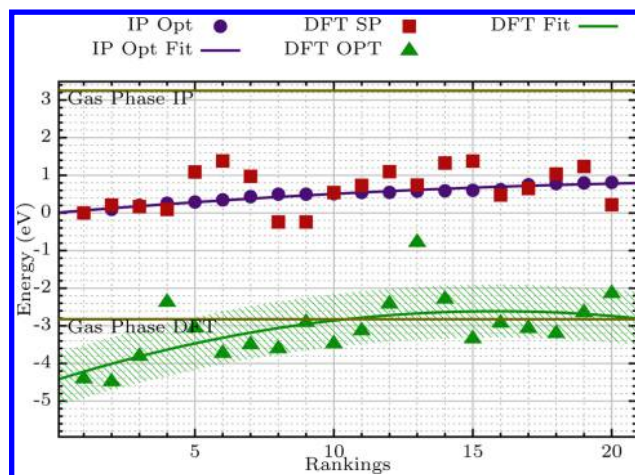


**Figure 10.** Relative  $\text{Cu}_{13}/\text{ZnO}$  energies of the lowest 20 IP structures as found by global optimization methods. Single-point and optimized DFT energies of the IP structures are shown as a comparison. Horizontal lines represent the relative energy of the  $\text{Cu}/\text{ZnO}$  systems when the gas-phase GM  $\text{Cu}_{13}$  cluster is dropped onto the surface and all ions are relaxed.

Energetically, when refined by DFT, the lowest energy structure is 0.32 eV lower in energy than the configuration obtained by relaxation of a gas-phase global minimum  $\text{Cu}_8$  cluster placed on top of the ZnO surface at ca. 3 Å (Figure 6); the atomic structures are different as seen in Figures 6 and 9. At the DFT level, only the second structure shown in Figure 9 is higher in energy than the one in Figure 6. Here, structurally, there is no substantial difference between IP and DFT (suggesting that this structure is either situated close to a local minima or it is very difficult to break its high symmetry); however, the energetic difference is 2.093 eV for DFT (when compared to the DFT GM); whereas for IP it is only 0.097 eV (Figure 9). The DFT optimized structures (Figure 9) reveal different atomic arrangements from those calculated with IP (not the case for the second structure), which makes direct comparison difficult between IP and DFT energies. The structural modification suggests that electrons play a significant role during the DFT refinement. We suggest a direct comparison by taking the relative IP energies of the optimized structures and those calculated with DFT, where the DFT energies are taken from a SP calculation on the optimized IP structures. The shifted SP DFT energies are 0.000,  $-0.430$ ,  $0.016$ ,  $-0.289$ , and  $-0.500$  eV. The second structure is very stable in comparison with the others, showing that the large mismatch is related to its positioning on the DFT landscape: it is very close to the bottom of the local minima, whereas the other four structures are further, thus allowing an additional energy gain of stabilisation.

Furthermore, we have investigated how well DFT determined structured map back onto the IP energy landscape. The  $\text{Cu}_n$  structures that we have obtained as minima on the DFT total energy landscape were used as starting points for a reoptimization with IP. Reassuringly, IP reoptimization has always resulted in one of already known local IP energy minima; that is, the search returned either to the global IP minimum or to a slightly higher energy state (Figure 9).

Structural and energetic discrepancies between the IP and DFT landscapes can be expected not only from our  $\text{Cu}-\text{ZnO}$  fit but also from parametrizations of the ZnO and/or  $\text{Cu}-\text{Cu}$  IP. Because the ZnO slab is held fixed and an excellent



agreement between the respective IP and DFT results has been proved earlier,<sup>40,62,88,100,101</sup> any mismatch should be linked to either the Cu–Cu or Cu–ZnO potentials. To rationalize further the behavior of the Cu/ZnO IP, we have calculated the self-energy of the five lowest energy IP structures shown in Figure 9, with the ZnO slab removed, using both IP and DFT. IP (DFT) self-energies, with respect to the first structure, are as follows: 0.000 eV (0.000 eV), 0.062 eV (0.345 eV), –1.387 eV (–0.942 eV), –0.261 eV (0.049 eV), and 0.442 eV (0.725 eV). On average, there is an energetic difference of ca. 0.3 eV between IP and DFT calculations. We note that the gas-phase Cu<sub>8</sub> IP and DFT energy landscapes show a preference for 3D clusters, whereas on the ZnO slab, the Cu clusters wet the surface, adopting flat configurations.

Next, we have assessed the self-energies of the corresponding gas-phase clusters obtained in our global optimization on the IP energy landscape of Cu<sub>8</sub>, using the periodic supercell model setup. The key concern has been whether the interaction of the clusters with their periodic images would significantly modify the energy landscape.

The results somewhat differ from the self-energies obtained for the supported clusters. IP (DFT) self-energies, with respect to the first structure, are as follows: 0.000 eV (0.000 eV), 0.534 eV (0.558 eV), –2.187 eV (–2.385 eV), –1.044 eV (–1.350 eV), and 0.506 eV (0.678 eV). Thus, as compared to the supported Cu<sub>8</sub> clusters, the gas-phase 3D clusters proved to be even more stable than the linear structures, which may be related to a further reduction in the coordination number. Again, there is a good agreement between IP and DFT energies with the greatest difference being ca. 0.3 eV (fourth structure, Figure 9) between the two approaches.

Another factor, which could cause a mismatch between IP and DFT calculations, is the inaccuracies of the fit between our Cu–ZnO potentials (Morse and Buckingham) and the calculated DFT data presented in Figure 3. Considering Figure 3, there are still small differences between the set of DFT data and our fit, which could be related to an insufficient flexibility of the Morse and Born–Mayer potentials employed (with only five variables in the parametric space).

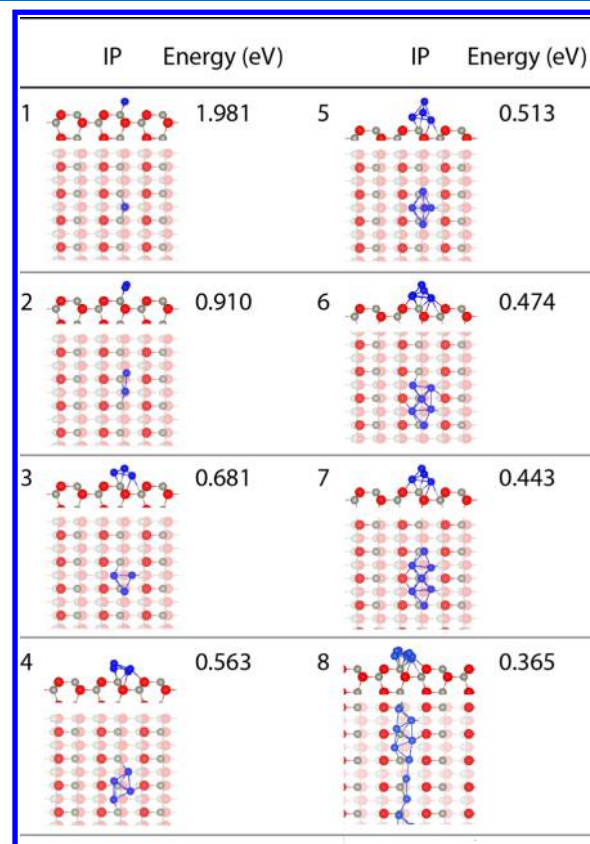
**Cu<sub>13</sub>/ZnO: An Energy Ranking Comparison between IP and DFT.** To analyze further the performance of our IP predicting low energy structures, we have refined the twenty lowest Cu<sub>13</sub>/ZnO IP structures using a DFT approach. Three different energies are analyzed: (i) IP energies of optimized structures, (ii) DFT SP energies from (i) structures, and (iii) DFT optimized energies from (ii). As discussed in the previous section, to compare DFT and IP energy landscape, the energy coming from the same atomic structure has to be used (i and ii).

Figure 10 shows energies (i–iii) for the Cu<sub>13</sub>/ZnO system. There are at least 14 structures, which are energetically more stable than the gas phase Cu<sub>13</sub> cluster interacting with the ZnO surface. The energetic difference between the gas-phase structure and those as predicted from global optimization techniques is up to 1.66 eV. The latter emphasizes the stronger need for the search of lower energy structures than those based on gas-phase GM clusters and also the power of global optimization techniques to perform this task.

Generally, our approach and potentials have proved to be very effective in predicting low energy Cu/ZnO with high accuracy and in performing global optimization calculations, which are unfeasible at the DFT level. Our calculations suggest that a small IP–DFT mismatch, caused by the landscape

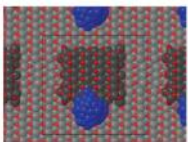
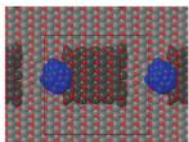
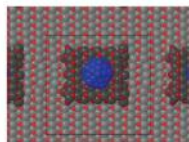
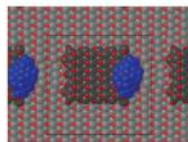




difference and the combination of simplifications in the Cu–Cu and Cu–ZnO potentials, must be expected. However, our potentials can filter low energy Cu/ZnO structures, suitable for a subsequent DFT refinement.

**Cu<sub>1–8</sub>/ZnO: An IP Analysis on the Structure and Energy.** In this section, we study growth of Cu<sub>n</sub> clusters (1 ≤ n ≤ 8) on the (10 $\bar{1}$ 0) surface at the IP level. Figure 11 shows the



**Figure 11.** Top and side views of the global minima found of Cu<sub>n</sub> clusters (1 ≤ n ≤ 8) deposited on the (4 × 3) (10 $\bar{1}$ 0) surface from global optimization. The formation energy (using Cu<sub>metal</sub> as a source of Cu) per Cu atom is displayed. n is displayed on the left of each figure.

GM structures and energies after global optimization for Cu<sub>n</sub>/ZnO. As copper and oxygen atoms are electron rich and zinc ions are poor, we expect a Cu–Zn attraction and a Cu–O repulsion. The latter behavior is observed in our calculations: Cu configurations tend to avoid oxygen atoms. Moreover, Cu triangular-based structures are predominant with a preference for planar Cu clusters. We calculated a decrease of the adsorption energy per Cu atom as the coverage increases, indicating a higher stability for bigger Cu clusters over the smaller ones. The higher stability for planar Cu clusters at low coverages is in agreement with STM studies by Dulub et al.<sup>102</sup> on the Zn-terminated (0001) ZnO surface, complemented by LEED, UPS, and LEIS. In general, a 2D copper growth is observed at low coverages (0.001–0.05 equiv ML), whereas at coverages greater than 0.01 ML, 3D clusters start to appear. As suggested earlier by STM images and quantum and molecular mechanical (QM/MM) calculations,<sup>26,37,102</sup> the ZnO substrate shows a strong influence on the Cu growth, as the 3D shape of the most stable gas-phase Cu clusters disappears when in contact with the ZnO surface. The preference for planar Cu

Adsorption site	A	B (O)	Terrace	B (Zn)
Top view				
Side view				
Energies (kJ mol <sup>-1</sup> )	40	38	23	44
Energies (J m <sup>-2</sup> )	2.22	2.59	1.80	2.65
Cu coverage (Å <sup>2</sup> )	167 (10%)	136 (8%)	122 (7.5%)	153 (9.5%)
Cu-Zn(O) Neighbours	54 (44)	46 (38)	29 (26)	42 (30)

**Figure 12.** Relaxed Cu<sub>55</sub>/ZnO structures for the different adsorption sites. Adsorption energies are given per Cu atom (kJ/mol) and per area (J/m<sup>2</sup>) at the bottom of each structure. Cu coverage in our simulation cell is given in Å<sup>2</sup> and in percentage. The number of Zn(O) nearest Cu neighbors with a cutoff distance of 3 Å is shown. Step B has two different terminations, Zn and O terminated, which are represented in parentheses. Dimensions of the Cu cluster, ZnO step, and simulation cell are given in Figure 7.

clusters at low coverages has been also found in a molecular dynamic study using COMB3 potentials.<sup>34</sup>

#### Cu Growth on Step Edges of the (10 $\bar{1}$ 0) Surface.

Following STM images by Dulub et al.<sup>21</sup> on the room-temperature growth of Cu on the (10 $\bar{1}$ 0) ZnO surface, we have studied these features using our Cu/ZnO IP. Experimentally, Cu nucleates in 3D structures with a prominent preference for the step edges perpendicular to the [1 $\bar{2}$ 0] atomic row direction. According to Dulub et al.,<sup>21</sup> the preferential Cu nucleation order on the (10 $\bar{1}$ 0) ZnO surface is along the (1 $\bar{2}$ 10) steps → on the terraces → along the (0001) steps.

The three different Cu<sub>55</sub> adsorption sites are displayed in Figure 7: site A (on a step edge perpendicular to the [1 $\bar{2}$ 0] direction), site B (on a step edge perpendicular to the [001] direction), and on a terrace. We note that step B has two different atomic configurations, Zn and O terminated. Figure 12 shows the relaxed atomic structures for Cu<sub>55</sub> adsorbed on the different sites. Adsorption energies per area are given as a comparison to previous energies reported experimentally<sup>103,104</sup> and theoretically<sup>37</sup> on Cu adsorption on ZnO polar surfaces. STM images<sup>21</sup> of pristine ZnO (10 $\bar{1}$ 0) surfaces show a high density of well-defined steps along the [1 $\bar{2}$ 0] and [001] direction. However, after Cu deposition, steps seem to go through strong atomic reconstructions, especially the one perpendicular to the polar [001] direction, which makes it difficult to simulate accurately. The adsorption energy per Cu atom on step edges is as follows: step B (44 kJ/mol, on the Zn terminated side), step A (40 kJ/mol), step B (38 kJ/mol, on the O terminated side), all of which are much higher than on a terrace (23 kJ/mol). We see that for the most stable case, Cu clusters tend to expand across the step and wet the surface, whereas the rest conserve a more 3D structure. The wetting increases the adsorption energy due to the higher number of Cu atoms interacting with the surface. However, adsorption on all sites is seen in experiment.

STM and HRTEM studies<sup>103,104</sup> of well-defined and clearly separated Cu clusters on the (0001) ZnO surface measured an adhesion work of Cu to the surface of  $3.4 \pm 0.1$  J/m<sup>2</sup>. Our IP calculated adsorption energies range from 1.80 to 2.65 J/m<sup>2</sup>,

implying that the adhesion work of Cu clusters on (10 $\bar{1}$ 0) ZnO surfaces is weaker than that on the Zn terminated (0001) ZnO surface.

To characterize the mode of adsorption, we have determined the coordination of Cu atoms to the surface, with coordination numbers (within a cutoff radius of 3 Å) shown in Figure 12. For the four different adsorption sites, the number of Cu–Zn bonds is greater, representing up to 58% of the total number of bonds. The average Cu coordination number (of the atoms in contact to the surface) to a Zn (O) atom is as follows: 2.25 (2.10) for site A, 2.19 (1.90) for site B (O), 1.93 (2.0) for terrace, and 2.21 (1.88) for site B (Zn). A radial distribution function is shown in Figure 13. The interaction between Cu atoms and surface Zn ions is characterized by a single strong peak at shorter distances and one or more weak satellites at significantly greater interatomic separations, that could be attributed to the high strength of the interaction, which is also the case for the interaction between Cu atoms in the cluster. For all adsorption sites, the nearest neighbor Cu–Zn interatomic distances are

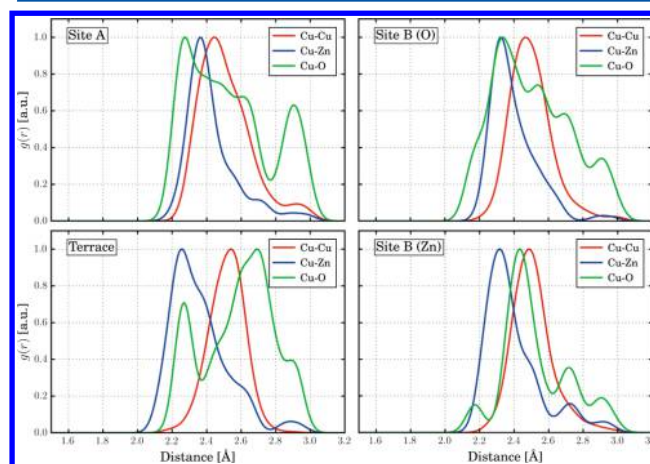


**Figure 13.** Radial distribution function plots for the four Cu adsorption sites comprising site A, site B (O), terrace, and site B (Zn).

shorter than the Cu–Cu distances, with the lowest Cu–Zn distance seen at the terrace. There is an anticorrelation between the Cu–Cu and Cu–Zn radial distributions. On the other hand, Cu–O interactions show multiple features. Sites A and B that expose oxygen to the interaction with adsorbates have a greater fraction of Cu–O interactions at shorter distances, as seen from the strong leading peak, which is accompanied by a set of shoulders and a weaker peak at about 2.9 Å. At the terrace and site B, the distribution inverts to a significantly weaker short distance and a much stronger mid-long distance with strong peaks. There is a clear differentiation among all sites. In general, at the base of the Cu cluster, inner atoms are bonded to three Zn ions, whereas the atoms in the circumference are bonded to two or one Zn ion. For the Cu–O interactions, the pattern is not as clear. For all of the adsorption sites, there are four characteristic peaks at ca. 2.25, 2.5, 2.65, and 2.9 Å. We recall that the Cu–O interaction is purely repulsive and any proximity of these species we observe should be due to the mediation role of the attractive Cu–Zn interaction, which could explain the greater spread of Cu–O distribution.

## SUMMARY AND CONCLUSIONS

We have parametrized IP that describe the interactions between copper clusters and zinc oxide surfaces. To obtain good quality Cu/ZnO IP, we have constructed a simulation model that enhances different aspects of Cu–ZnO interactions, including (i) bulk-like nonpolar ZnO surface terminations, which maximize the accessibility of surface ions of both kinds; (ii) planar Cu<sub>4</sub> and 3D Cu<sub>8</sub> clusters with closed-shell electronic configuration; and (iii) Born–Mayer and Morse potentials, which gave a good description of the repulsive Cu–O and attractive Cu–Zn interactions, respectively.

We have achieved a good fit of the IP to DFT SP calculations, which is the basis for reliable modeling of the Cu/ZnO system. Optimizing this procedure, we have found that the relaxation of the ZnO has no substantial effect on the Cu<sub>8</sub> structures, which can be exploited to speed up global optimization searches or similar stochastic calculations.

Our global optimization calculations of Cu<sub>8</sub> directly on the ZnO surface found three structures lower in energy than the structure obtained by adsorbing on the (10 $\bar{1}$ 0) surface the gas-phase GM Cu<sub>8</sub> cluster, with the largest difference of 0.32 eV.

Considering the atomic structure, a close similarity between IP and DFT results was achieved with the IP showing some preference for planar Cu structures. In most cases, the DFT optimized structures were found in less than 40 ionic steps starting from preoptimized IP configurations, whereas calculations using the same computational resources and the gas-phase GM Cu<sub>8</sub> cluster 3 Å above the ZnO surface as a starting point can take over 200 ionic steps. Overall, the new Cu/ZnO IP proved to give a good structural agreement with DFT calculations.

Cu adsorption energies, in general, are in a good agreement between IP and DFT levels of theory. However, we observed a strong disagreement for the second lowest energy supported Cu<sub>8</sub> structure. This result is related to the difference between energy IP and DFT landscapes: it is very close to a local minimum on the DFT energy landscape, which is why its atomic arrangement does not change substantially, whereas the other four structures relax further. There is a small energy IP–DFT mismatch, which is produced by the combination of inaccuracies in the Cu–Cu and Cu–ZnO potentials. We note

that the Cu–ZnO potentials were fitted using only five parameters, which might produce a relatively simple IP that is not sufficient to describe well such a complex system.

In agreement with previous experimental and theoretical work on the polar ZnO surfaces, global optimizations of Cu<sub>n</sub> clusters ( $1 \leq n \leq 7$ ) deposited on the (10 $\bar{1}$ 0) surface show a preference for planar Cu clusters, with a strong attraction between the Cu and Zn species, which determines the morphology of supported clusters.

We have provided the first theoretical study on the stabilization of Cu nanoparticles on the step edges of the nonpolar ZnO (10 $\bar{1}$ 0) surface. The Cu wetting on the step edges increases the adsorption energy due to the higher number of Cu atoms interacting with the substrate. However, adsorption on all sites is seen in experiment.

The methodology presented here provides a very good approximation to the structure and energy of the Cu/ZnO system and allows us to sample a substantial representative portion of the potential energy landscape in a reasonable amount of time. From this process, the lowest energy IP structures can be selected as candidates for refinement with an *ab initio* method. Our methodology can be easily transferred to study any supported nanocluster systems in the search of the thermodynamically most stable nanocluster/substrate structure and to study large systems, which are usually required for modeling nanocluster growth on substrates. Obtaining the lowest energy structure for such systems is, usually, a difficult task due to the large number of possible configurations (on the order of thousands), a task that, until now, goes beyond the DFT capabilities. The methodology shown in this Article provides a successful and unbiased way to find these low energy structures without any precondition.

## AUTHOR INFORMATION

### Corresponding Authors

\*E-mail: david.fonz.11@ucl.ac.uk.

\*E-mail: a.sokol@ucl.ac.uk.

### ORCID

David Mora-Fonz: 0000-0002-0310-9891

Tomas Lazauskas: 0000-0002-8351-9857

Stefan T. Bromley: 0000-0002-7037-0475

Alexey A. Sokol: 0000-0003-0178-1147

### Notes

The authors declare no competing financial interest.

## ACKNOWLEDGMENTS

UK Catalysis Hub is kindly thanked for resources and support provided via our membership of the UK Catalysis Hub Consortium and funded by EPSRC (grants EP/K014706/2, EP/K014668/1, EP/K014854/1, EP/K014714/1, and EP/M013219/1). We are thankful for funding from EPSRC (EP/L000202, EP/I03014X, EP/K038958, and EP/K000144) and Mexican sponsors (CONACYT, SEP, UJAT); for HPC facilities from UK's ARCHER and UCL's Legion and Grace (Legion@UCL and Grace@UCL); and for useful discussions with J. C. Schön, I. Demiroglu, J. Buckeridge, M. R. Farrow, D. O. Scanlon, and S. A. Shevlin. STB acknowledges financial support from Spanish MINECO/FEDER grant CTQ2015-64618-R and, in part, by Generalitat de Catalunya (grants 2014SGR97 and XRQTC).

## REFERENCES

- (1) Waugh, K. C. Methanol Synthesis. *Catal. Lett.* **2012**, *142*, 1153–1166.
- (2) Chinchin, G.; Denny, P.; Parker, D.; Spencer, M.; Whan, D. Mechanism of Methanol Synthesis from CO<sub>2</sub>/CO/H<sub>2</sub> Mixtures over Copper/Zinc Oxide/Alumina Catalysts: Use of <sup>14</sup>C-Labelled Reactants. *Appl. Catal.* **1987**, *30*, 333–338.
- (3) Bowker, M.; Hadden, R.; Houghton, H.; Hyland, J.; Waugh, K. The Mechanism of Methanol Synthesis on Copper/Zinc Oxide/Alumina Catalysts. *J. Catal.* **1988**, *109*, 263–273.
- (4) Ressler, T.; Kniep, B. L.; Kasatkin, I.; Schlögl, R. The Microstructure of Copper Zinc Oxide Catalysts: Bridging the Materials Gap. *Angew. Chem., Int. Ed.* **2005**, *44*, 4704–4707.
- (5) Waller, D.; Stirling, D.; Stone, F. S.; Spencer, M. S. Copper/Zinc Oxide Catalysts. Activity in Relation to Precursor Structure and Morphology. *Faraday Discuss. Chem. Soc.* **1989**, *87*, 107–120.
- (6) Günter, M.; Ressler, T.; Jentoft, R.; Bems, B. Redox Behavior of Copper Oxide/Zinc Oxide Catalysts in the Steam Reforming of Methanol Studied by in Situ X-Ray Diffraction and Absorption Spectroscopy. *J. Catal.* **2001**, *203*, 133–149.
- (7) Behrens, M.; Studt, F.; Kasatkin, I.; Kühl, S.; Hävecker, M.; Abild-Pedersen, F.; Zander, S.; Girgsdies, F.; Kurr, P.; Kniep, B.-L.; Tovar, M.; Fischer, R. W.; Nørskov, J. K.; Schlögl, R. The Active Site of Methanol Synthesis over Cu/ZnO/Al<sub>2</sub>O<sub>3</sub> Industrial Catalysts. *Science* **2012**, *336*, 893–7.
- (8) Behrens, M.; Kasatkin, I.; Kuhl, S.; Weinberg, G. Phase-Pure Cu,Zn,Al Hydrotalcite-like Materials as Precursors for Copper Rich Cu/ZnO/Al<sub>2</sub>O<sub>3</sub> Catalysts. *Chem. Mater.* **2010**, *22*, 386–397.
- (9) Müller, M.; Hermes, S.; Kähler, K.; van den Berg, M. W. E.; Muhler, M.; Fischer, R. A. Loading of MOF-5 with Cu and ZnO Nanoparticles by Gas-Phase Infiltration with Organometallic Precursors: Properties of Cu/ZnO@MOF-5 as Catalyst for Methanol Synthesis. *Chem. Mater.* **2008**, *20*, 4576–4587.
- (10) Breen, J. P.; Ross, J. R. Methanol Reforming for Fuel-Cell Applications: Development of Zirconia-Containing Cu-Zn-Al Catalysts. *Catal. Today* **1999**, *51*, 521–533.
- (11) Spencer, M. S. The Role of Zinc Oxide in Cu/ZnO Catalysts for Methanol Synthesis and the Water–gas Shift Reaction. *Top. Catal.* **1999**, *8*, 259–266.
- (12) U. of York. Methanol. 2014; <http://www.essentialchemicalindustry.org/chemicals/methanol.html> [accessed November 2016].
- (13) Bowker, M.; Houghton, H.; Waugh, K. C. Mechanism and Kinetics of Methanol Synthesis on Zinc Oxide. *J. Chem. Soc., Faraday Trans. 1* **1981**, *77*, 3023–3036.
- (14) Waugh, K. Methanol Synthesis. *Catal. Today* **1992**, *15*, 51–75.
- (15) Yoshihara, J.; Parker, S.; Campbell, C. Island Growth Kinetics During Vapor Deposition of Cu onto the Zn-Terminated ZnO(0001) Surface. *Surf. Sci.* **1999**, *439*, 153–162.
- (16) Møller, P. J.; Nerlov, J. Ultrathin Films of Cu on ZnO(1120): Growth and Electronic Structure. *Surf. Sci.* **1994**, *307*, 591–596.
- (17) Bech, M.; Simonsen, J. B.; Handke, B.; Li, Z.; Møller, P. J. Copper Nucleation on ZnO(1120) in the Presence of Sulphur. *Surf. Sci.* **2006**, *600*, 3375–3381.
- (18) Ernst, K. H.; Ludviksson, A.; Zhang, R.; Yoshihara, J.; Campbell, C. T. Growth Model for Metal Films on Oxide Surfaces: Cu on ZnO(0001)-O. *Phys. Rev. B: Condens. Matter Mater. Phys.* **1993**, *47*, 13782–13796.
- (19) Yoshihara, J.; Campbell, J.; Campbell, C. Cu Films on a Zn-Terminated ZnO(0001) Surface: Structure and Electronic Properties. *Surf. Sci.* **1998**, *406*, 235–245.
- (20) Harikumar, K.; Santra, A. A Comparative Study of the Interaction of CO with Cu and Cu-Zn Alloy Clusters. *Solid State Commun.* **1996**, *99*, 403–406.
- (21) Dulub, O.; Boatner, L. A.; Diebold, U. STM Study of Cu Growth on the ZnO(1010) Surface. *Surf. Sci.* **2002**, *504*, 271–281.
- (22) Patterson, M. C.; Nie, X.; Wang, F.; Kurtz, R. L.; Sinnott, S. B.; Asthagiri, A.; Sprunger, P. T. Growth and Structure of Cu and Au on the Nonpolar ZnO(1010) Surface: STM, XPS, and DFT Studies. *J. Phys. Chem. C* **2013**, *117*, 18386–18397.
- (23) Ozawa, K.; Sato, T.; Oba, Y.; Edamoto, K. Electronic Structure of Cu on ZnO(1010): Angle-Resolved Photoemission Spectroscopy Study. *J. Phys. Chem. C* **2007**, *111*, 4256–4263.
- (24) Didziulis, S. V.; Butcher, K. D.; Cohen, S. L.; Solomon, E. I. Chemistry of Copper Overlayers on Zinc Oxide Single-Crystal Surfaces: Model Active Sites for Copper/Zinc Oxide Methanol Synthesis Catalysts. *J. Am. Chem. Soc.* **1989**, *111*, 7110–7123.
- (25) Derrouiche, S.; Lauron-Pernot, H.; Louis, C. Synthesis and Treatment Parameters for Controlling Metal Particle Size and Composition in Cu/ZnO Materials-First Evidence of Cu<sub>3</sub>Zn Alloy Formation. *Chem. Mater.* **2012**, *24*, 2282–2291.
- (26) Catlow, C. R. A.; French, S. A.; Sokol, A. A.; Alfredsson, M.; Bromley, S. T. Understanding the Interface Between Oxides and Metals. *Faraday Discuss.* **2003**, *124*, 185–203.
- (27) Catlow, C.; French, S.; Sokol, A.; Thomas, J. Computational Approaches to the Determination of Active Site Structures and Reaction Mechanisms in Heterogeneous Catalysts. *Philos. Trans. R. Soc., A* **2005**, *363*, 913–936.
- (28) French, S.; Sokol, A.; Bromley, S.; Catlow, C.; Sherwood, P. Identification and Characterization of Active Sites and Their Catalytic Processes-the Cu/ZnO Methanol Catalyst. *Top. Catal.* **2003**, *24*, 161–172.
- (29) Rasmussen, D. B.; Janssens, T. V.; Temel, B.; Bligaard, T.; Hinnemann, B.; Helveg, S.; Sehested, J. The Energies of Formation and Mobilities of Cu Surface Species on Cu and ZnO in Methanol and Water Gas Shift Atmospheres Studied by DFT. *J. Catal.* **2012**, *293*, 205–214.
- (30) Bromley, S. T.; French, S. A.; Sokol, A. A.; Catlow, C. R. A.; Sherwood, P. Metal Cluster Support Interactions in the Cu/ZnO System: A QM/MM Study. *J. Phys. Chem. B* **2003**, *107*, 7045–7057.
- (31) Yang, L.; Karim, A.; Muckerman, J. T. Density Functional Kinetic Monte Carlo Simulation of Water–Gas Shift Reaction on Cu/ZnO. *J. Phys. Chem. C* **2013**, *117*, 3414–3425.
- (32) Hellström, M.; Spångberg, D.; Hermansson, K.; Broqvist, P. Small Cu Clusters Adsorbed on ZnO(1010) Show Even–Odd Alternations in Stability and Charge Transfer. *J. Phys. Chem. C* **2014**, *118*, 6480–6490.
- (33) Cheng, Y.-T.; Shan, T.-R.; Devine, B.; Lee, D.; Liang, T.; Hinojosa, B. B.; Phillpot, S. R.; Asthagiri, A.; Sinnott, S. B. Atomistic Simulations of the Adsorption and Migration Barriers of Cu Adatoms on ZnO Surfaces Using COMB Potentials. *Surf. Sci.* **2012**, *606*, 1280–1288.
- (34) Cheng, Y.-T.; Liang, T.; Nie, X.; Choudhary, K.; Phillpot, S. R.; Asthagiri, A.; Sinnott, S. B. Cu Cluster Deposition on ZnO(1010): Morphology and Growth Mode Predicted from Molecular Dynamics Simulations. *Surf. Sci.* **2014**, *621*, 109–116.
- (35) Hu, H.; Lv, Z.; Cui, S.; Zhang, G. Theoretical Study of ZnO(1010) and M/ZnO(1010) (M = Cu, Ag and Au) Surfaces with DFT Approach. *Chem. Phys. Lett.* **2011**, *510*, 99–103.
- (36) Beltrán, A.; Andrés, J.; Calatayud, M.; Martins, J. Theoretical Study of ZnO (1010) and Cu/ZnO (1010) Surfaces. *Chem. Phys. Lett.* **2001**, *338*, 224–230.
- (37) French, S. A.; Sokol, A. A.; Catlow, C. R. A.; Sherwood, P. The Growth of Copper Clusters over ZnO: the Competition between Planar and Polyhedral Clusters. *J. Phys. Chem. C* **2008**, *112*, 7420–7430.
- (38) Hellström, M.; Spångberg, D.; Hermansson, K.; Broqvist, P. Cu Dimer Formation Mechanism on the ZnO(1010) Surface. *Phys. Rev. B: Condens. Matter Mater. Phys.* **2012**, *86*, 235302 1–8.
- (39) Scarano, D.; Spoto, G.; Bordiga, S.; Zecchina, A.; Lamberti, C. Lateral Interactions in CO Adlayers on Prismatic ZnO Faces: a FTIR and HRTEM Study. *Surf. Sci.* **1992**, *276*, 281–298.
- (40) Mora-Fonz, D.; Buckeridge, J.; Logsdail, A. J.; Scanlon, D. O.; Sokol, A. A.; Woodley, S.; Catlow, C. R. A. Morphological Features and Band Bending at Nonpolar Surfaces of ZnO. *J. Phys. Chem. C* **2015**, *119*, 11598–11611.

- (41) Mora-Fonz, D.; Lazauskas, T.; Farrow, M. R.; Catlow, C. R. A.; Woodley, S. M.; Sokol, A. A. Why Are Polar Surfaces of ZnO Stable? *Chem. Mater.* **2017**, *29*, 5306–5320.
- (42) Coleman, V. A.; Jagadish, C. *Zinc Oxide Bulk, Thin Film. Nanostructures*; Elsevier: New York, 2006; pp 1–20.
- (43) Look, D. C.; Claffin, B. P-Type Doping and Devices Based on ZnO. *Phys. Status Solidi B* **2004**, *241*, 624–630.
- (44) Özgür, U.; Alivov, Y. I.; Liu, C.; Teke, A.; Reshchikov, M. A.; Dogan, S.; Avrutin, V.; Cho, S.-J.; Morkoc, H. A. Comprehensive Review of ZnO Materials and Devices. *J. Appl. Phys.* **2005**, *98*, 041301 1–103.
- (45) Pearton, S. Recent Progress in Processing and Properties of ZnO. *Prog. Mater. Sci.* **2005**, *50*, 293–340.
- (46) Farrow, M. R.; Buckeridge, J.; Lazauskas, T.; Mora-Fonz, D.; Scanlon, D. O.; Catlow, C. R. A.; Woodley, S. M.; Sokol, A. A. Heterostructures of GaN with SiC and ZnO Enhance Carrier Stability and Separation in Framework Semiconductors. *Phys. Status Solidi A* **2017**, *214*, 1600440 1–7.
- (47) Parker, T.; Condon, N.; Lindsay, R.; Leible, F.; Thornton, G. Imaging the Polar (000 $\bar{1}$ ) and Non-Polar (10 $\bar{1}$ 0) Surfaces of ZnO with STM. *Surf. Sci.* **1998**, *415*, L1046–L1050.
- (48) Jedrecy, N.; Gallini, S.; Sauvage-Simkin, M.; Pinchaux, R. The ZnO Non-Polar (10 $\bar{1}$ 0) Surface: An X-Ray Structural Investigation. *Surf. Sci.* **2000**, *460*, 136–143.
- (49) Klenov, D. O.; Kryukova, G. N.; Plyasova, L. M. Localization of Copper Atoms in the Structure of the ZnO Catalyst for Methanol Synthesis. *J. Mater. Chem.* **1998**, *8*, 1665–1669.
- (50) Hu, J.; Guo, W.-P.; Shi, X.-R.; Li, B.-R.; Wang, J. Copper Deposition and Growth over ZnO Nonpolar (10 $\bar{1}$ 0) and (11 $\bar{2}$ 0) Surfaces: A Density Functional Theory Study. *J. Phys. Chem. C* **2009**, *113*, 7227–7235.
- (51) Liang, T.; Shan, T.-R.; Cheng, Y.-T.; Devine, B. D.; Noordhoek, M.; Li, Y.; Lu, Z.; Phillpot, S. R.; Sinnott, S. B. Classical Atomistic Simulations of Surfaces and Heterogeneous Interfaces with the Charge-Optimized Many Body (COMB) Potentials. *Mater. Sci. Eng., R* **2013**, *74*, 255–279.
- (52) Kau, L. S.; Hodgson, K. O.; Solomon, E. I. X-Ray Absorption Edge and EXAFS Study of the Copper Sites in Zinc Oxide Methanol Synthesis Catalysts. *J. Am. Chem. Soc.* **1989**, *111*, 7103–7109.
- (53) Günter, M.; Ressler, T.; Bems, B.; Büscher, C.; Genger, T.; Hinrichsen, O.; Muhler, M.; Schlögl, R. Implication of the Microstructure of Binary Cu/ZnO Catalysts for their Catalytic Activity in Methanol Synthesis. *Catal. Lett.* **2001**, *71*, 37–44.
- (54) Klier, K. *Advances in Catalysis*; Academic Press: New York, 1982; pp 243–313.
- (55) Mehta, S.; Simmons, G.; Klier, K.; Herman, R. Catalytic Synthesis of Methanol from CO<sub>2</sub>: II. Electron Microscopy (TEM, STEM, Microdiffraction, and Energy Dispersive Analysis) of the CuZnO and Cu/ZnO/Cr<sub>2</sub>O<sub>3</sub> Catalysts. *J. Catal.* **1979**, *57*, 339–360.
- (56) Meitzner, G.; Iglesia, E. New Insights into Methanol Synthesis Catalysts from X-Ray Absorption Spectroscopy. *Catal. Today* **1999**, *53*, 433–441.
- (57) Jansen, W. Dynamic Behavior of the Surface Structure of Cu/ZnO/SiO<sub>2</sub> Catalysts. *J. Catal.* **2002**, *210*, 229–236.
- (58) Batyrev, E. D.; Shiju, N. R.; Rothenberg, G. Exploring the Activated State of Cu/ZnO(0001)-Zn, a Model Catalyst for Methanol Synthesis. *J. Phys. Chem. C* **2012**, *116*, 19335–19341.
- (59) Batyrev, E.; van den Heuvel, J.; Beckers, J.; Jansen, W.; Castricum, H. The Effect of the Reduction Temperature on the Structure of Cu/ZnO/SiO<sub>2</sub> Catalysts for Methanol Synthesis. *J. Catal.* **2005**, *229*, 136–143.
- (60) Vilhelmsen, L. B.; Hammer, B. Systematic Study of Au<sub>6</sub> to Au<sub>12</sub> Gold Clusters on MgO(100) F Centers Using Density-Functional Theory. *Phys. Rev. Lett.* **2012**, *108*, 126101.
- (61) Ferrando, R.; Rossi, G.; Nita, F.; Barcaro, G.; Fortunelli, A. Interface-Stabilized Phases of Metal-on-Oxide Nanodots. *ACS Nano* **2008**, *2*, 1849–1856.
- (62) Demiroglu, I.; Woodley, S. M.; Sokol, A. A.; Bromley, S. T. From Monomer to Monolayer: a Global Optimisation Study of (ZnO)<sub>n</sub> Nanoclusters on the Ag Surface. *Nanoscale* **2014**, *6*, 14754–65.
- (63) Brookes, C.; Wells, P. P.; Dimitratos, N.; Jones, W.; Gibson, E. K.; Morgan, D. J.; Cibir, G.; Nicklin, C.; Mora-Fonz, D.; Scanlon, D. O.; Catlow, C. R. A.; Bowker, M. The Nature of the Molybdenum Surface in Iron Molybdate. The Active Phase in Selective Methanol Oxidation. *J. Phys. Chem. C* **2014**, *118*, 26155–26161.
- (64) Logsdail, A. J.; Scanlon, D. O.; Catlow, C. R. A.; Sokol, A. A. Bulk Ionization Potentials and Band Alignments From Three-Dimensional Periodic Calculations as Demonstrated on Rocksalt Oxides. *Phys. Rev. B: Condens. Matter Mater. Phys.* **2014**, *90*, 155106 1–8.
- (65) Logsdail, A. J.; Mora-Fonz, D.; Scanlon, D. O.; Catlow, C. R. A.; Sokol, A. A. Structural, Energetic and Electronic Properties of (100) Surfaces for Alkaline Earth Metal Oxides as Calculated with Hybrid Density Functional Theory. *Surf. Sci.* **2015**, *642*, 58–65.
- (66) Posada Borbon, A. The Structure of Metal-Oxide Interfaces Investigated by Genetic Algorithms. Ph.D. Thesis, Chalmers University of Technology, 2016.
- (67) Artrith, N.; Hiller, B.; Behler, J. Neural Network Potentials for Metals and Oxides - First Applications to Copper Clusters at Zinc Oxide. *Phys. Status Solidi B* **2013**, *250*, 1191–1203.
- (68) Göpel, W.; Pollmann, J.; Ivanov, I.; Reihl, B. Angle-Resolved Photoemission from Polar and Nonpolar Zinc Oxide Surfaces. *Phys. Rev. B: Condens. Matter Mater. Phys.* **1982**, *26*, 3144–3150.
- (69) Dulub, O.; Boatner, L. A.; Diebold, U. STM Study of the Geometric and Electronic Structure of ZnO(0001)-Zn, (000 $\bar{1}$ )-O, (10 $\bar{1}$ 0), and (11 $\bar{2}$ 0) Surfaces. *Surf. Sci.* **2002**, *519*, 201–217.
- (70) Kresse, G.; Dulub, O.; Diebold, U. Competing Stabilization Mechanism for the Polar ZnO(0001)-Zn Surface. *Phys. Rev. B: Condens. Matter Mater. Phys.* **2003**, *68*, 245409 1–15.
- (71) Goniakowski, J.; Finocchi, F.; Noguera, C. Polarity of Oxide Surfaces and Nanostructures. *Rep. Prog. Phys.* **2008**, *71*, 016501 1–55.
- (72) Cheng, Y.-T.; Liang, T.; Martinez, J. A.; Phillpot, S. R.; Sinnott, S. B. A Charge Optimized Many-Body Potential for Titanium Nitride (TiN). *J. Phys.: Condens. Matter* **2014**, *26*, 265004 1–12.
- (73) Cheng, Y.-T.; Shan, T.-R.; Liang, T.; Behera, R. K.; Phillpot, S. R.; Sinnott, S. B. Optimized Many-Body (comb) Potential for Titanium and Titania. *J. Phys.: Condens. Matter* **2014**, *26*, 315007 1–12.
- (74) Shan, T.-R.; Devine, B. D.; Kemper, T. W.; Sinnott, S. B.; Phillpot, S. R. Charge-Optimized Many-Body Potential for the Hafnium/Hafnium Oxide System. *Phys. Rev. B: Condens. Matter Mater. Phys.* **2010**, *81*, 125328 1–12.
- (75) Shan, T.-R.; Devine, B. D.; Phillpot, S. R.; Sinnott, S. B. Molecular Dynamics Study of the Adhesion of Cu/SiO<sub>2</sub> Interfaces using a Variable-Charge Interatomic Potential. *Phys. Rev. B: Condens. Matter Mater. Phys.* **2011**, *83*, 115327 1–8.
- (76) Liang, T.; Shin, Y. K.; Cheng, Y.-T.; Yilmaz, D. E.; Vishnu, K. G.; Verners, O.; Zou, C.; Phillpot, S. R.; Sinnott, S. B.; van Duin, A. C. Reactive Potentials for Advanced Atomistic Simulations. *Annu. Rev. Mater. Res.* **2013**, *43*, 109–129.
- (77) Raymand, D.; van Duin, A. C.; Goddard, W. A.; Hermansson, K.; Spångberg, D. Hydroxylation Structure and Proton Transfer Reactivity at the Zinc Oxide-Water Interface. *J. Phys. Chem. C* **2011**, *115*, 8573–8579.
- (78) Raymand, D.; van Duin, A. C.; Spångberg, D.; Goddard, W. A.; Hermansson, K. Water Adsorption on Stepped ZnO Surfaces from MD Simulation. *Surf. Sci.* **2010**, *604*, 741–752.
- (79) Mueller, J. E.; van Duin, A. C. T.; Goddard, W. A. Development and Validation of ReaxFF Reactive Force Field for Hydrocarbon Chemistry Catalyzed by Nickel. *J. Phys. Chem. C* **2010**, *114*, 4939–4949.
- (80) Lazauskas, T.; Sokol, A. A.; Woodley, S. M. An Efficient Genetic Algorithm for Structure Prediction at the. *Nanoscale* **2017**, *9*, 3850–3864.
- (81) Kresse, G.; Hafner, J. Ab Initio Molecular-Dynamics Simulation of the Liquid-Metal-Amorphous-Semiconductor Transition in Germa-

nium. *Phys. Rev. B: Condens. Matter Mater. Phys.* **1994**, *49*, 14251–14269.

(82) Kresse, G.; Furthmüller, J. Efficiency of Ab-Initio Total Energy Calculations for Metals and Semiconductors using a Plane-Wave Basis Set. *Comput. Mater. Sci.* **1996**, *6*, 15–50.

(83) Perdew, J.; Ruzsinszky, A.; Csonka, G.; Vydrov, O.; Scuseria, G.; Constantin, L.; Zhou, X.; Burke, K. Restoring the Density-Gradient Expansion for Exchange in Solids and Surfaces. *Phys. Rev. Lett.* **2008**, *100*, 136406 1–4.

(84) Blöchl, P. E. Projector Augmented-Wave Method. *Phys. Rev. B: Condens. Matter Mater. Phys.* **1994**, *50*, 17953–17979.

(85) Kresse, G. From Ultrasoft Pseudopotentials to the Projector Augmented-Wave Method. *Phys. Rev. B: Condens. Matter Mater. Phys.* **1999**, *59*, 1758–1775.

(86) Gale, J. D. GULP: A Computer Program for the Symmetry-Adapted Simulation of Solids. *J. Chem. Soc., Faraday Trans.* **1997**, *93*, 629–637.

(87) Gale, J. D.; Rohl, A. L. The General Utility Lattice Program (GULP). *Mol. Simul.* **2003**, *29*, 291–341.

(88) Whitmore, L.; Sokol, A. A.; Catlow, C. R. A. Surface Structure of Zinc Oxide (10 $\bar{1}$ 0), using an Atomistic, Semi-Infinite Treatment. *Surf. Sci.* **2002**, *498*, 135–146.

(89) Cleri, F.; Rosato, V. Tight-Binding Potentials for Transition Metals and Alloys. *Phys. Rev. B: Condens. Matter Mater. Phys.* **1993**, *48*, 22–33.

(90) Woodley, S. M. Knowledge Led Master Code Search for Atomic and Electronic Structures of LaF<sub>3</sub> Nanoclusters on Hybrid Rigid Ion-Shell Model-DFT Landscapes. *J. Phys. Chem. C* **2013**, *117*, 24003–24014.

(91) Farrow, M. R.; Chow, Y.; Woodley, S. M. Structure Prediction of Nanoclusters; A Direct or a Pre-Screened Search on the DFT Energy Landscape? *Phys. Chem. Chem. Phys.* **2014**, *16*, 21119–21134.

(92) Darby, S.; Mortimer-Jones, T. V.; Johnston, R. L.; Roberts, C. Theoretical Study of Cu-Au Nanoalloy Clusters Using a Genetic Algorithm. *J. Chem. Phys.* **2002**, *116*, 1536–1550.

(93) Rusina, G. G.; Borisova, S. D.; Chulkov, E. V. Structure and Analysis of Atomic Vibrations in Clusters of Cu<sub>n</sub> ( $n \leq 20$ ). *Russ. J. Phys. Chem. A* **2013**, *87*, 233–239.

(94) Gafner, Y. Y.; Gafner, S. L.; Zamulin, I. S.; Redel, L. V.; Baidyshev, V. S. Analysis of the Heat Capacity of Nanoclusters of FCC Metals on the Example of Al, Ni, Cu, Pd, and Au. *Phys. Met. Metallogr.* **2015**, *116*, 568–575.

(95) Chepkasov, I. V.; Redel, L. V. Calculations of the Heat Capacity of Cu Clusters Synthesized by Condensation from the Gas Phase. *IOP Conf. Ser.: Mater. Sci. Eng.* **2015**, *81*, 012014 1–5.

(96) Wilson, N. T. Ph.D. Thesis, University of Birmingham, 2000.

(97) D'Agostino, G. Copper Clusters Simulated by a Many-Body Tight-Binding Potential. *Philos. Mag. B* **1993**, *68*, 903–911.

(98) Erkoç; Shaltaf, R. Monte Carlo Computer Simulation of Copper Clusters. *Phys. Rev. A: At, Mol., Opt. Phys.* **1999**, *60*, 3053–3057.

(99) Jug, K.; Zimmermann, B.; Calaminici, P.; Köster, A. M. Structure and Stability of Small Copper Clusters. *J. Chem. Phys.* **2002**, *116*, 4497–4507.

(100) Sokol, A. A.; French, S. A.; Bromley, S. T.; Catlow, C. R. A.; van Dam, H. J. J.; Sherwood, P. Point Defects in ZnO. *Faraday Discuss.* **2007**, *134*, 267–282.

(101) Al-Sunaidi, A. A.; Sokol, A. A.; Catlow, C. R. A.; Woodley, S. M. Structures of Zinc Oxide Nanoclusters: As Found by Revolutionary Algorithm Techniques. *J. Phys. Chem. C* **2008**, *112*, 18860–18875.

(102) Dulub, O.; Batzill, M.; Diebold, U. Growth of Copper on Single Crystalline ZnO: Surface Study of a Model Catalyst. *Top. Catal.* **2005**, *36*, 65–76.

(103) Koplitz, L. V.; Dulub, O.; Diebold, U. STM Study of Copper Growth on ZnO(0001)-Zn and ZnO(000 $\bar{1}$ )-O Surfaces. *J. Phys. Chem. B* **2003**, *107*, 10583–10590.

(104) Hansen, P. L. Atom-Resolved Imaging of Dynamic Shape Changes in Supported Copper Nanocrystals. *Science* **2002**, *295*, 2053–2055.